Volume 41

http://acousticalsociety.org/



18th International Symposium on Long Range Sound Propagation

3-4 August 2020

Computational Acoustics: LRSP 2020

Multi-year regional infrasound detection of Tungurahua, El Reventador, and Sangay volcanoes in Ecuador from 2006 to 2013

Hugo D. Ortiz

Department of Earth Science and Earth Research Institute; University of California, Santa Barbara, CA, USA; Facultad de Ciencias Exactas y Naturales; Pontificia Universidad Católica del Ecuador, Quito, 170525, ECUADOR; huda013@gmail.com; hdortiz@ucsb.edu

Robin S. Matoza, Charusheela Garapaty and Kaelynn Rose

Department of Earth Science and Earth Research Institute; University of California, Santa Barbara, Santa Barbara, CA, USA; rmatoza@ucsb.edu; garapaty@ucsb.edu; kaelynn@ucsb.edu

Patricio Ramón and Mario C. Ruiz

Instituto Geofísico, Escuela Politécnica Nacional, Quito, Pichincha, ECUADOR; pramon@igepn.edu.ec; mruiz@igepn.edu.ec

As part of the Acoustic Surveillance for Hazardous Eruptions project, two infrasound arrays were installed in northern and central Ecuador. The RIOE and LITE arrays were operational between 2006 and 2013, recording thousands of infrasound signals originating from eruptions of Tungurahua, El Reventador, and Sangay. We use Progressive Multi-Channel Correlation array processing together with hierarchical clustering to identify and associate impulsive infrasound signals with each volcano. Infrasound detections correspond to quasi-continuous activity of Sangay between mid 2006 and mid 2012, at least thirteen periods of activity of Tungurahua between 2006 and mid 2012, and strong signals from El Reventador in early 2008. We validate our detections using satellite observations from the MODIS (Moderate Resolution Imaging Spectroradiometer) volcano detection algorithm (MODVOLC) and independent eruption catalogs. For Sangay, we find a good agreement between our infrasound detections and MODVOLC triggers, whereas for El Reventador the agreement is fair. We attribute the fair correspondence at El Reventador to the low-temporal resolution of MODIS data and frequent cloud cover in the region that reduce satellite observational capability. Finally, our study highlights the benefits of infrasound arrays for monitoring volcanoes in Ecuador at regional distances, while further investigating the processes that limit volcanic infrasound detection.



1. INTRODUCTION

A rapid expansion of infrasound technology started at the beginning of the century with the installation of infrasound arrays and networks for local, regional, and global monitoring of volcanoes and nuclear tests (Matoza et al. 2019; and references therein). Multiple studies have demonstrated the potential utility of infrasound technology for detecting, locating, and characterizing signals not only from volcanoes and nuclear explosions, but also from microbaroms, tsunamis, earthquakes, snow avalanches, meteorites, rivers, waterfalls, chemical explosions, mine blasts, supersonic flights, wind farms, surf, etc. (Le Pichon et al. 2019; and references therein). As a result, infrasound technology has become highly complementary to seismic studies and vice versa (e.g., Arrowsmith et al., 2010; Hedlin et al., 2012); leading to joint seismic and infrasound sensor networks that show promise for improved geophysical monitoring (e.g., Matoza et al., 2018; Shani-Kadmiel et al, 2018; Wilson et al., 2018). Two of the most prominent examples of such installations are the International Monitoring System (e.g., Marty, 2019) and the EarthScope Transportable Array, US (e.g., Sanderson et al., 2020). A recent trend has also been toward the development of low-cost instrumentation (Marcillo et al. 2012; Anderson et al. 2018; Ortiz et al. 2018; Grangeon and Lesage, 2019) and enabling findable, accessible, interoperable, and reusable (FAIR) data (e.g., Fee et al., 2020; Anderson et al., 2020). At present, the seismic and infrasonic research community has access to an expanding archive of digital waveform data from around the globe spanning decades, motivating the investigation of data mining methods that utilize machine learning for increased automation (e.g. Kong et al. 2019; Anzieta et al. 2019).

Previous studies applying machine learning to infrasound datasets have largely focused on classifying signals from different natural and anthropogenic sources (e.g. Albert and Linville 2020; Li et al. 2016). The majority of the studies used supervised machine learning to classify signals and benchmark methods using existing catalogs from the International Monitoring System (IMS) International Data Center (IDC) and subsidiaries (e.g. Ham and Park, 2002; Park et al. 2005; Liu et al. 2014; Li et al. 2016; Albert and Linville 2020). For instance, Liu et al. (2014) and Li et al. (2016) applied support vector machine to a catalog of 139 events comprising signals from earthquakes, volcanoes, and tsunamis and obtained classification accuracies of ~97% and ~86%, respectively. Then Albert and Linville (2020) extended the analysis using support vector machine and convolutional neural networks to a dataset which consisted of 519 events recorded at multiple stations and included signals from mines and quarries, chemical explosions, earthquakes, and volcanoes. For the more complex dataset, Albert and Linville (2020) obtained classification accuracies of ~55%. On the other hand, fewer studies have used unsupervised machine learning to classify infrasound signals. Ruiz et al. (2006) selected 28 explosion events from Tungurahua and applied principal component analysis to group the signals depending in waveform similarity. Cannata et al. (2011) used Density-Based Spatial Clustering with Noise to group activity from different vents and to label the type of volcanic activity at Mount Etna. Witsil and Johnson (2020) used kmeans clustering to continuous infrasound recordings to identify shifts in volcanic behavior of Stromboli and in a similar approach Watson (2020) applied k-means clustering to label different eruptive phases of Mt. Etna. Cannata et al. (2011) used ~665 events, and Witsil and Johnson (2020) and Watson (2020) used three days of continuous data for the clustering algorithms.

Here, we apply unsupervised machine learning to a multiyear infrasound dataset from 2006 to 2013 to investigate periods of eruptive activity at volcanoes Tungurahua, Sangay, and El Reventador in Ecuador. We apply hierarchical clustering following Ward's criterion (Ward, 1963) to group impulsive short-lived signals from these volcanoes parsed from array processing coherent infrasound detection lists. We use the detections of the impulse signals to characterize the quasi-continuous activity of Sangay, at least thirteen periods of activity of Tungurahua, and a strong eruption of El Reventador in early 2008.

2. THE ACOUSTIC SURVEILLANCE FOR HAZARDOUS ERUPTIONS (ASHE) PROJECT

Two 4-element infrasound arrays, LITE and RIOE, were installed in early 2006 in northern and central Ecuador in the Andes (Fig. 1a) and remained active until the beginning of 2013 as part of the Acoustic Surveillance for Hazardous Eruptions (ASHE) project (Garcés et al. 2008; Fee et al. 2010). The goal of the

project was to issue low-latency bulletins to the Volcanic Ash Advisory Centers about eruptions that could pose a risk to aviation in the region (see Matoza et al., 2019 for a review). Each infrasound array consisted of four Chaparral 2.5 microphones with a flat frequency response between 0.1 and 200 Hz connected to 24-bit Trident digitizer. The signals were sampled at 40 Hz and sent in real-time via Satellite to the Geological Survey of Canada. The apertures of the arrays were ~120 m and ~150 m for LITE and RIOE, respectively (Fig. 1b).

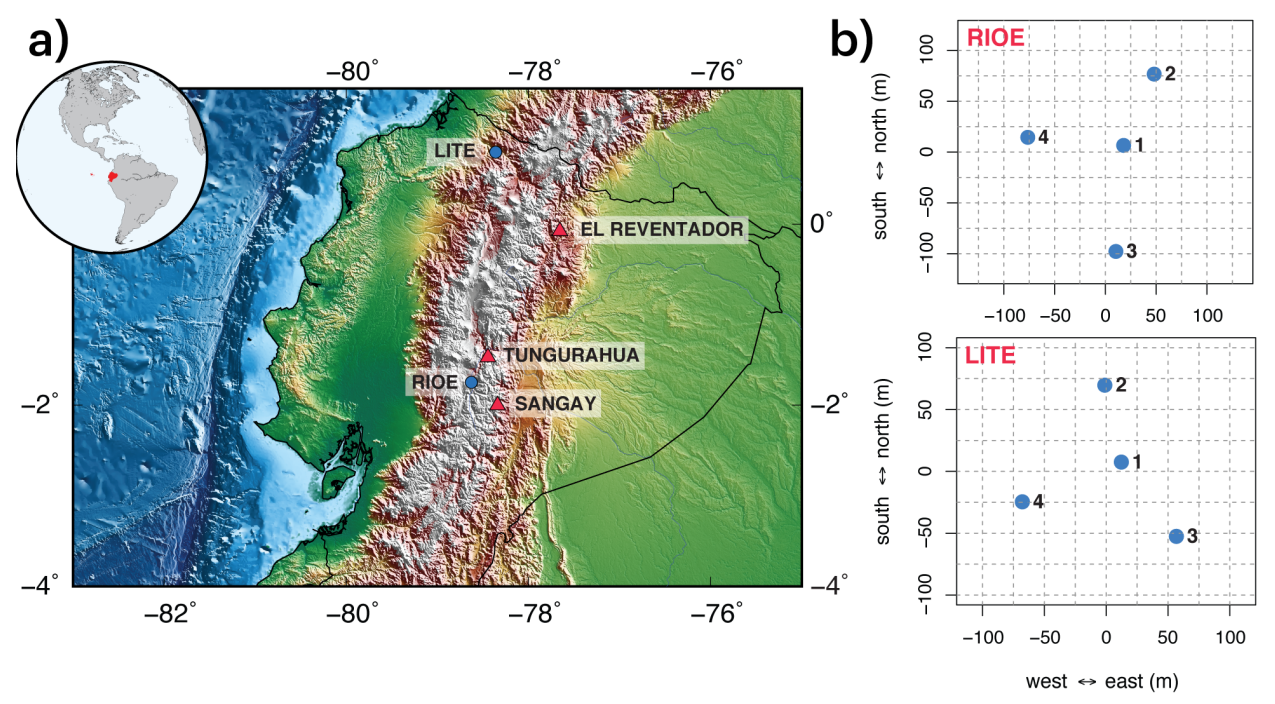


Figure 1. Infrasound arrays and major active volcanoes in Ecuador. a) In 2006, as part of the Acoustic Surveillance for Hazardous Eruptions (ASHE) project, LITE and RIOE infrasound arrays were installed in northern and central Ecuador over the Andes to monitor hazardous eruptions from volcanoes that included El Reventador, Tungurahua, and Sangay. b) The LITE and RIOE infrasound arrays were each composed of 4 infrasound sensors with apertures of ~120 m and 150 m, respectively. The LITE and RIOE arrays remained fully operational (four sensors working simultaneously) until 15 October 2011 and 7 May 2012, respectively.

Existing studies that used ASHE data have only focused on eruptions of Tungurahua between 2006 and 2010 (e.g. Garcés et al. 2008; Fee et al. 2010; Matoza et al. 2009; Assink et al. 2012). For instance, Fee et al. (2010) provided the chronology and characterization of Tungurahua eruptive activity between 2006 and 2008 using the RIOE array. Assink et al. (2012) used impulsive infrasonic signals from Tungurahua recorded at LITE during August 2006, February 2008, and June 2010 to probe the sensitivity of their travel times to atmospheric tides. Matoza et al. (2009) and Matoza et al. (2013) characterized energetic-continuous infrasonic tremor recorded at RIOE in 2006 and 2008 as a low-frequency form of jet noise produced by man-made jets (see Matoza and Fee, 2018). Matoza and Fee (2014) studied the coupling of infrasonic tremor down into the ground for the 14–15 July 2006 eruption of Tungurahua using data recorded at RIOE. Finally, Matoza et al. (2014) highlighted the diverse nature of waveform characteristics of explosions of Tungurahua recorded between 2006 and 2008 at RIOE. Here we reprocess the ASHE dataset between 2006 and 2013 to obtain eruption catalogs of Tungurahua, Sangay, and El Reventador. A summary of distances and back azimuths between the arrays and volcanoes is provided in Table 1.

Table 1. Distances and back azimuths between arrays and volcanoes. We follow the definition of Matoza et al. (2018) and refer to local (<15 km), regional (15-250 km), and remote (>250 km) source-receiver ranges.

	Tungurahua	Sangay	El Reventador
RIOE	37 km; 33°	43 km; 132°	214 km; 30°
LITE	251 km; 182°	310 km; 179°	124 km; 140°

3. METHODS

In this section is described how we 1) detect coherent signals recorded in the arrays, 2) cut time-series and prepare signals, 3) compute the dissimilarity matrix for the signals, and 4) cluster the impulsive signals.

A. DETECTION AND SIGNAL CONDITIONING

To obtain the direction of arrival of coherent infrasound signals recorded at the arrays, we use the time-domain Progressive Multi-Channel Correlation method (PMCC; Cansi,1995). The general idea of PMCC is to find a slowness vector compatible with time delays between microphones of a coherent (correlated) signal crossing the array under a plane-wave assumption over several frequency bands, windows lengths, and microphone triads (e.g. Cansi and Le Pichon, 2008). In this study, we use 15 log-spaced frequency bands and time-window lengths, a similar configuration to the one presented by Matoza et al. (2017). The windows are consecutive with an overlap of 10% of the window length. The ~4.3 million PMCC family detections for RIOE between 2006 and 2013 show diverse infrasound sources (Fig. 2). Frequent sources include Sangay, El Reventador, and Tungurahua volcanoes, microbaroms arriving from the Pacific Ocean, and (presumably) anthropogenic noise.

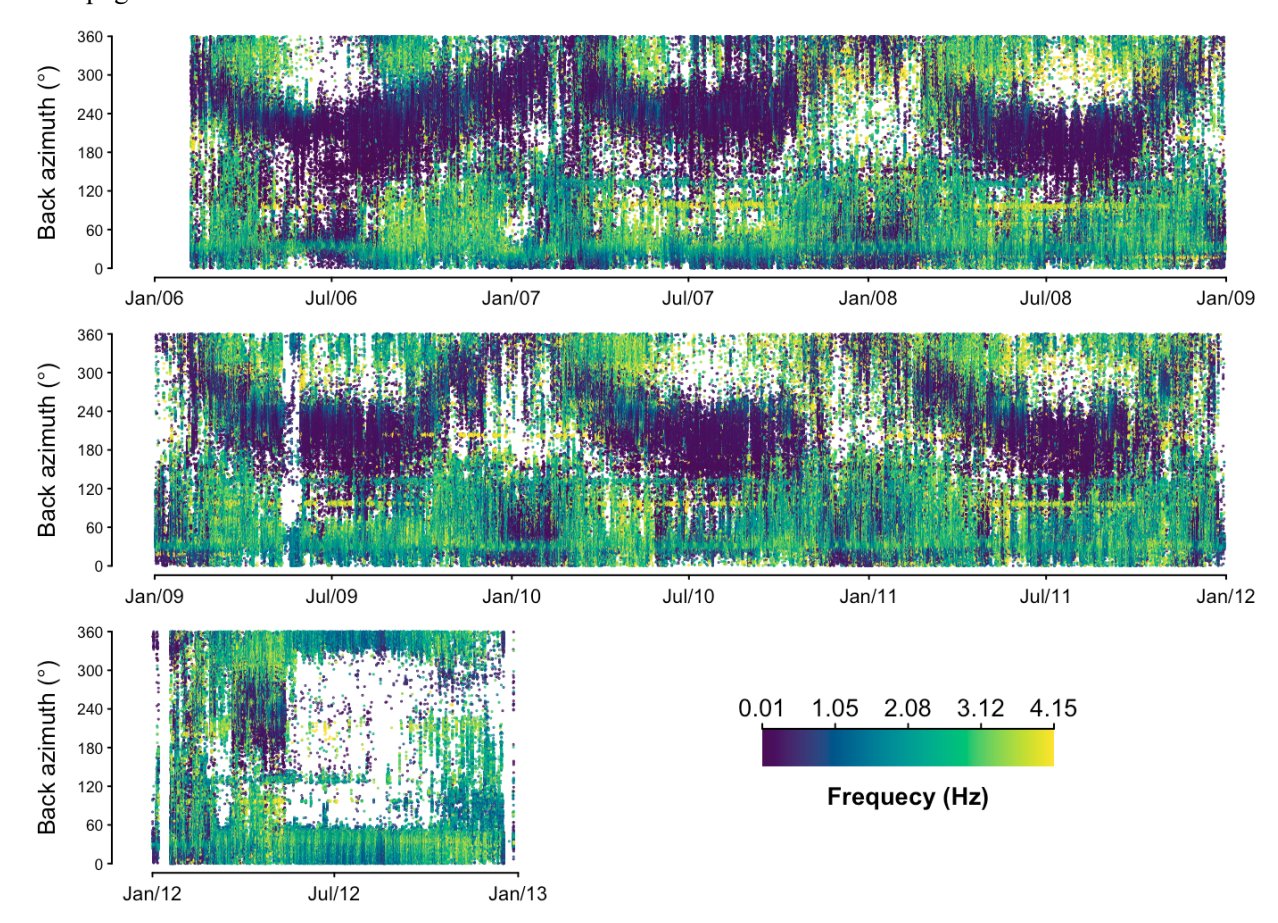


Figure 2. PMCC detections for the RIOE array from 2006 to 2013 plotted as arrival back azimuth vs. time and color coded for mean detection frequency. Frequent infrasound detections are interpreted as microbaroms (~180°–360°; < 0.7 Hz), Sangay (~132°; 1–3 Hz), anthropogenic noise (~96°; > 3.5 Hz), and Tungurahua and El Reventador (~ 31.5°; 1-3 Hz). The detection capability is diminished on 7 May 2012, after a malfunction of array element (sensor) #4.

Once we have the multi-year PMCC catalog, which includes signal onset times, we choose a subset of detections within the expected back azimuth of the source that we attempt to classify. For example, for Tungurahua, we select signals with back azimuths of $33^{\circ} \pm 10^{\circ}$ to allow some room for azimuth variability from cross winds during propagation and for back azimuth estimation error which is typically ~5° for common infrasound array configurations (Szuberla and Olson, 2004). Subsequently, we cut the signals in a two-stage process. First, we detrend and filter the signals using a 4-order Butterworth filter between 1 and 4 Hz because

most of the volcanic detections are in this frequency band as shown in Fig. 2. Second, we cut the signals using windows of length 51.2 s (2048 samples) starting at the PMCC onset time. We repeat the cutting process for each microphone and stack the traces to improve the signal-to-noise ratio. We save the stacked trace to the disk for later use in the clustering process.

B. CLUSTERING AND CATALOG

We cluster the stacked signals in a two-stage process to reduce computational burden. In the first stage, we divide the multiyear catalog into bins of 15 days, totaling 25 bins per year. Next, we compute the cross-correlation coefficients for all signal-pairs within a 15-day bin to build the cross-correlation matrix C, from which we compute the dissimilarity matrix d, as:

$$d = 1 - |C| \tag{1}$$

We then apply hierarchical clustering following Ward's criterion (Ward, 1963; see Appendix A) to each d, allowing 30 distinct clusters. For each cluster, we align and stack the waveforms to obtain a single master waveform.

In the second stage, we merge and grow the clusters by year. For instance, in 2008 there are 750 (30 clusters * 25 bins) master waveforms (Fig. 3). We again compute the cross-correlation coefficients for all pair combinations and obtain a new dissimilarity matrix, which we use to group the master waveforms into 20 clusters following the Ward's criterion. In this stage, we reduce the number of clusters from 30 to 20 because the number of signals to be grouped also decreases by about two orders of magnitude, thus making the data processing more efficient and still allowing the convergence of enough distinct groups. Finally, we visually inspect the master waveforms and corresponding clusters to choose the impulsive short-lived infrasonic signals. In the example depicted in Fig. 3, we select master waveforms in groups 1, 3, 5, 8, 13 and corresponding cluster members as the final yearly catalog. We repeat the process for each year, from 2006 to 2012.

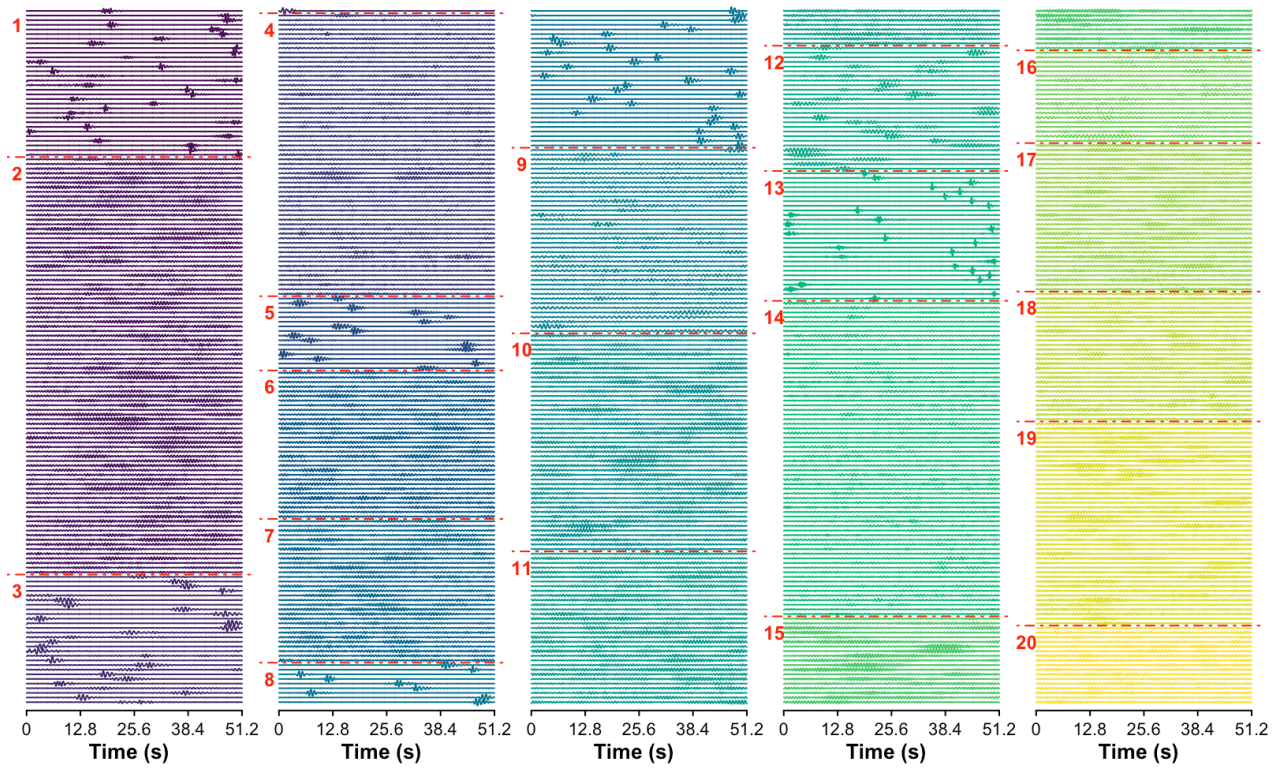


Figure 3. Summary of master waveforms retrieved in 2008. Each column has 150 waveforms, totaling 750 waveforms, which are divided into 20 group following the hierarchical clustering under the Ward's criterion. Horizontal red lines mark the limits between clusters. Impulsive signals appear in groups 1, 3, 5, 8, and 13.

4. RESULTS

For Tungurahua, we start with 2,101,169 detections with azimuths between 23° and 43° during the seven years of data (Fig. 4a). After cleaning the initial catalog utilizing hierarchical clustering, we obtain a total of 351,838 transient short-lived explosions at RIOE (Fig. 4b). We refer to the initial detection catalog as "preliminary" (Fig. 4a), and the catalog after applying the clustering algorithm as "clean" (Fig. 4b). In the clean catalog, we identify at least thirteen periods of elevated (> 350 daily detections) acoustic activity of Tungurahua: 11 February – 17 August 2006, 10–12 October 2006, 2–18 March 2007, 24 October 2007 – 14 February 2008, 22 May 2008, 8-9 November 2008, 20 December 2008 - 24 February 2009, 5-23 June 2009, 31 December 2009 -19 February 2010, 27 May 2010 - 7 June 2010, 22 November - 10 December 2010, 20 April - 18 May 2011, and 27 November 2011 – 24 July 2012. For comparison, we present explosion detections carried out by analysts at Instituto Geofisico (IG) (the local volcano monitoring agency in Ecuador) using a set of sensors in proximity (< 5 km) to Tungurahua (Fig. 4c). Analysts visually inspect seismic and infrasound records to find and catalog impulsive signals whose travel times coincide with signals originating at the Tungurahua vent region. For additional comparison, we also display hotspot detections of the MODIS (Moderate Resolution Imaging Spectroradiometer) volcano detection algorithm (MODVOLC; Wright et al., 2002 and 2004) from 2006 until 2013 (horizontal red bar in Fig. 4). MODVOLC detections are triggered when thermal anomalies are found in the MODIS Level 1B images taken by the Aqua and Terra satellites. MODIS images have a spatial resolution of up to 1 km and a temporal resolution of at least 2 days.

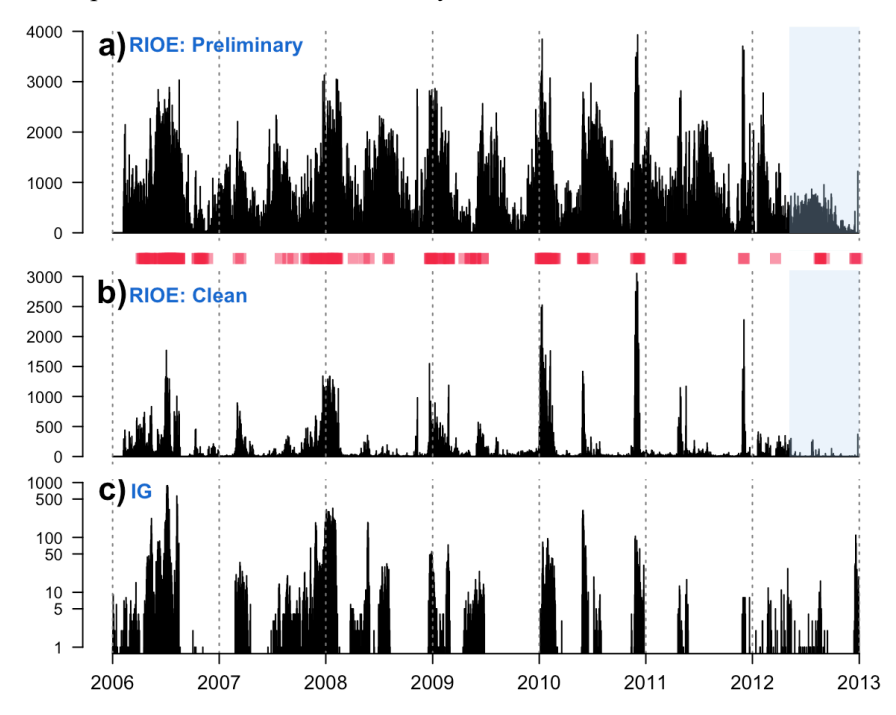


Figure 4. "Preliminary", "clean", and analyst catalogs of Tungurahua signals from 2006 to 2013. a) The number of daily PMCC detections at RIOE for azimuths between 23° and 43° are 2,101,169 and it is referred as the preliminary catalog. b) Daily count of impulsive signals found after applying hierarchical clustering and the Ward's criterion is referred as the clean catalog. The 351, 838 impulsive signals show at least thirteen periods with detections greater than 350 per day. c) Analyst detections of impulsive signals using the local monitoring network run by Instituto Geofisico (IG). The semi-transparent red squares between panels a and b represent MODVOLC detections. The more red a square is the more MODVOLC detections there are. In panels a and b, the blue shadow areas indicate that only 3 microphones are working simultaneously.

As for Sangay and El Reventador, we follow an analogous process as the one described in Section 3 for Tungurahua. The differences are that for Sangay we select PMCC detections at RIOE with back azimuths of $132^{\circ} \pm 12^{\circ}$, whereas for El Reventador we pick PMCC detections at LITE (the closest array) with back azimuths of $140^{\circ} \pm 15^{\circ}$. Back azimuth deviations can also occur for these detections as winds play an important role during infrasound propagation. We permit greater back azimuth deviations at Sangay and El Reventador because the

source-receiver distance is greater than Tungurahua's source-receiver distance, especially for El Reventador which is 124 km away from LITE (Table 1).

We begin with 72,306 and 193,960 detections for Sangay and El Reventador, respectively, between 2006 and 2013 (Fig. 5). Since the initial number of detections is considerably smaller than for Tungurahua, we use one bin per year for Sangay and a total of 25 bins for El Reventador during the seven years. From here, the procedure repeats. For each bin, we compute the dissimilarity matrix, and find 30 distinct groups using hierarchical clustering in combination with the Ward's criterion. Finally, to obtain multi-year catalogs, we merge and grow the clusters by visually selecting the impulsive signals. We find a total of 19,726 and 11,375 impulsive transient infrasound signals for Sangay (Fig. 5a) and El Reventador (Fig. 5b), respectively. There is no local infrasound monitoring from 2006 to 2013 for neither Sangay or El Reventador, therefore we only present the MODVOLC detections for comparison. (horizontal red bars in Fig. 5).

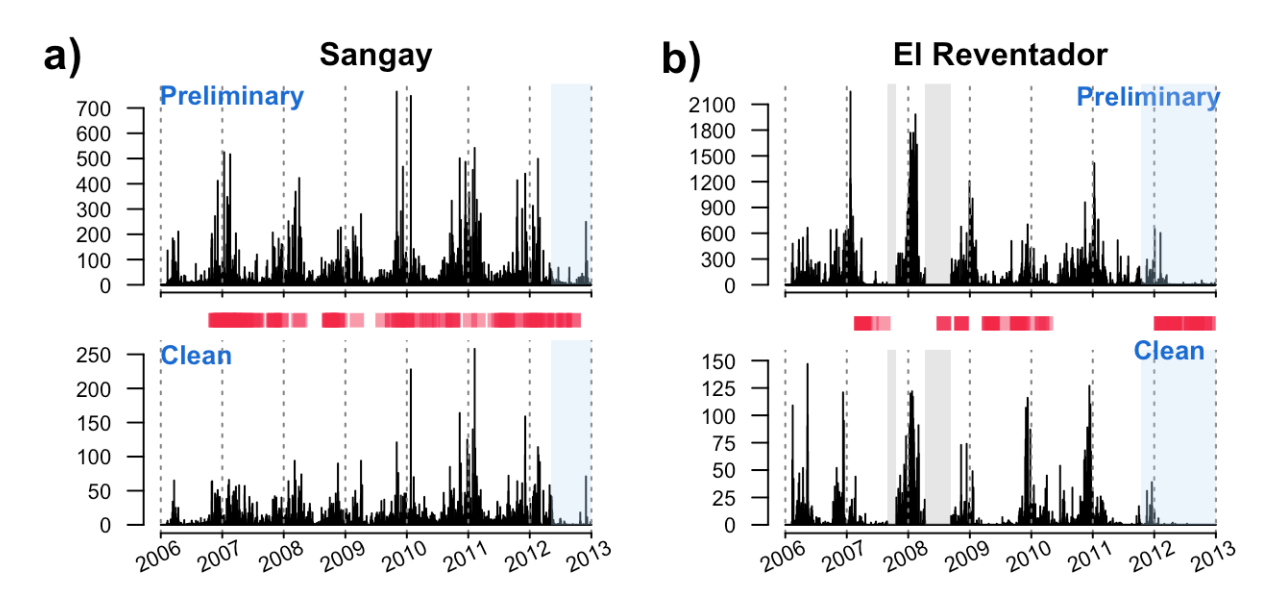


Figure 5. "Preliminary" and "clean" daily infrasound detections (vertical black lines) compared to MOVOLC hotspot detections (horizontal red bars) for Sangay and El Reventador. a) There are 72,306 preliminary detections between 120° and 144° at RIOE. Once we clean the initial dataset through hierarchical clustering, we find 19,726 impulsive signals coming from the direction of Sangay. The MODVOLC detections show a good agreement with the periods of high infrasound activity. b) We start with 193,960 detections at LITE with back azimuths of 125°-155°. Then we find 11,375 impulsive signals arriving from the direction of El Reventador. A fair agreement between daily infrasound and MODVOLC detections is reasonable, since satellite monitoring is challenging in the area due to heavy cloud cover. The blue shaded areas indicate that only 3 microphones are working simultaneously, while gray shaded areas indicate that data are not available.

5. DISCUSSION

A. TUNGURAHUA

The infrasound detections presented in Fig. 4b closely resemble the Instituto Geofisico catalog of explosions (Fig. 4c), suggesting that our method can be used to characterize the eruptive periods of Tungurahua at regional distances with a single array. Between 2006 and 2013, we recognize at least thirteen periods of activity with detections greater than 350 per day that also coincide with eruption reports of previous studies (Arellano et al. 2008; Garcés et al., 2008; Fee et al., 2010; Mothes et al., 2015; Hidalgo et al., 2015; Ortiz et al., 2018) as well as with MODVOLC detections (Fig. 4). The eruptive activity of Tungurahua was intermittent, with eruptions of strombolian, vulcanian, and sub-Plinian nature. From 2006 to 2010, eruptions were mainly of strombolian nature in combination with some energetic vulcanian episodes. However, there are two large pyroclastic forming eruptions in July and August 2006 (Arellano et al., 2008). Starting in 2010, the activity on average was more

intense than in previous years. This mostly consisted of vulcanian eruptions that produced small pyroclastic flows and sometimes strong infrasonic activity that was audible at up to 30 km from Tungurahua (Mothes et al., 2015; Ortiz et al., 2018).

B. SANGAY

Sangay is one of the most active andesitic volcanoes in the world with eruption reports starting as early as 1628 (Monzier et al., 1999). Eleven large eruptions are summarized by Monzier et al. (1999) from 1628 to 1942, along with the evolution of the activity and morphology of Sangay from 1950 to 1995. The activity has been diverse with surficial manifestations such us lava flows, multi-vent activity, ash emissions, pyroclastic density currents, debris flows, and rockfalls (Monzier et al., 1999; Robles, 2010). The most recent infrasound studies at Sangay (Johnson and Lees, 2000; Lees and Ruiz, 2008) mainly focused on characterizing a type of harmonic tremor known as chugging, using data from a campaign lasting 5 days in April 1998.

Since Sangay is located in a remote area in challenging terrain, the volcano has been poorly instrumented and most of its activity has occurred without local (<15 km) continuous geophysical monitoring. Here we present (Fig. 5a) a first multi-year characterization of detections of infrasound activity of Sangay between 2006 and 2013. In this case, we benchmark our infrasound detections with MODVOLC hot spot detections (Fig. 5a) and visual reports of activity. Infrasound at RIOE show near-constant activity from mid 2006 to mid 2012, with 8 detections per day in average and a maximum of 258 detections in 8 February of 2011. The reported infrasound activity agrees with the MODVOLC detections from 2007 to 2013 and are consistent with the visual records presented by Robles (2010) between 2007 and 2010. We identify three periods of relatively low infrasound activity in 25 April – 25 October 2006, 12 June – 11 August 2008, and 11 April – 1 Jul 2009 that correspond to not detections from MODVOLC. This is expected as hot spots may not be registered due to the weak activity of Sangay that may has been shadowed by the frequent clouds in the area or the low temporal resolution of the satellite data used by MODVOLC.

C. EL REVENTADOR

In November 2002, a violent eruption destroyed the upper volcanic edifice of El Reventador, producing pyroclastic density currents that traveled up to 9 km from the summit (Hall et al. 2004). From 2002 to 2020, tens of lava flows and pyroclastic deposits have reconstructed the volcanic cone twice (Naranjo et al., 2016; Arnold et al., 2017 and 2019; Eruption Reports of Instituto Geofisico, www.igepn.edu.ec). Until 2015, the volcanic cone was already in a similar shape to the one before November 2002. This rapid growth led to instabilities and morphological changes in the upper part of the edifice. Between early 2015 and mid 2018, these changes were photo-documented by Almeida and Gaunt (2019) and highlighted by three main processes: the opening of a new vent during 2015, a flank eruption in June 2017, and partial summit collapse in April 2018. The rapid extrusive activity at El Reventador continues and volcanic deposits have already filled up the scarp that resulted from the collapse in 2018.

Continuous local infrasound monitoring of El Reventador started in early 2013, recording frequent impulsive signals and, less commonly, sustained long-lived (tremor) signals (Ortiz et al. 2019; Ortiz et al., 2021; Eruption Reports of Instituto Geofisico). The accompanying infrasound activity of El Reventador is persistent and of variable size with eruptions of strombolian and vulcanian character (Naranjo et al., 2016; Ortiz et al. 2019; Ortiz et al., 2021).

We provide the infrasound activity chronology of El Reventador registered at LITE, between 2006 and 2013 (Fig. 5b). On average, there are 5 detections per day and a maximum of 147 detections in 13 May 2006. We expect lower number of detections of El Reventador because the source-receiver range is 124 km, corresponding to a typical stratospheric shadow zone. We also benchmark our infrasound detections with MODVOLC hot spot detections, giving a fair agreement (at least the eruptions in 2009 and 2010 appear in both catalogs). As highlighted by Naranjo et al. (2016), satellite monitoring in the area is especially hard to achieve because lava flows and pyroclastic deposits are frequently covered by clouds. For example, following a cross bearings approach using both arrays (e.g. Matoza et al., 2017), we confirm that during peak detections from 1 January to

22 February 2008 the signals localize at El Reventador, even though there are not MODVOLC triggers (Fig. 6). This highlights the utility of infrasound as a ground-based regional geophysical monitoring technique for this volcano (e.g., Matoza and Fee, 2018).

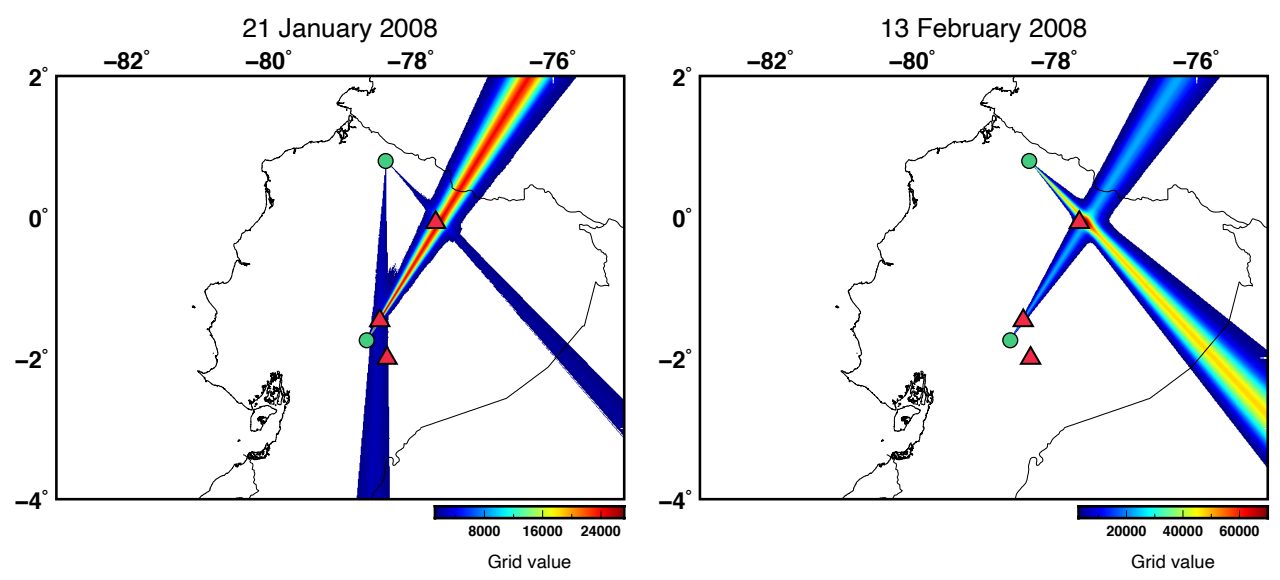


Figure 6. Snapshots of the cross-bearings approach for 21 January and 13 February 2008. Warmer colors indicate increased number of backprojected infrasound detection back azimuths. On 21 January 2008, LITE and RIOE infrasound arrays (green circles) indicate that the origins of the signals are at El Reventador and Tungurahua volcanoes (red triangles). On 13 February 2008, both infrasound arrays point to a single infrasound source at El Reventador. We record clear continuous infrasound signals from El Reventador; however, there are not MODVOLC triggers for the period 1 January – 22 February 2008.

D. METHOD

We investigate the capability of unsupervised machine learning applied to a large infrasound data set to find impulsive signals originating at Tungurahua, Sangay, and El Reventador from 2006 to 2013. We find good correspondence between our regional infrasound detection catalog and the local infrasound catalog of Tungurahua (Figs. 4b-c). For Sangay, there is a good agreement between infrasound detections and MODVOLC triggers, whereas for El Reventador the agreement is fair (Fig. 5). We attribute the fair correspondence at El Reventador to reduced satellite monitoring capability, as the area is often covered by clouds. Consequently, the results suggest that applying hierarchical clustering with Ward's criterion can improve the detection capability from standard single infrasound array techniques.

Apart from the spectral characteristics of the sounds generated by each volcano, three other major factors broadly affect our ability to characterize the impulsive signals: separation between arrays and volcanoes (source-receiver range), the size of eruptions, and wind noise. Unsurprisingly, the number of impulsive infrasound detections decreases as a function range. We find a higher number of impulsive signals for Tungurahua given its proximity (37 km) to RIOE and its frequent large amplitude explosions that were often reported. Sangay is also relatively close (43 km) to RIOE, where we record almost continuous impulsive signals. There are no clear arrivals from Sangay at 314 km range at LITE, and Sangay signals already register with relatively low signal-to-noise at RIOE. We obtain fewer detections of impulsive signals attributable to El Reventador at LITE given the 124 km range. However, emergent signals attributable to El Reventador are frequently recorded at both LITE and RIOE. Lastly, we observe considerably fewer PMCC detections during daytime than nighttime at both arrays. Turbulent fluctuations of the air are enhanced by the incoming sun radiation leading to stronger wind noise levels at daytime (e.g., Walker and Hedlin, 2010). Thereby, wind noise highly reduces our ability to characterize weak signals with low signal-to-noise ratios during daytime at regional distances.

6. CONCLUSION

We present the first regional infrasound detection catalogs for Tungurahua, Sangay, and El Reventador from 2006 to 2013. The catalogs are especially useful for reconstructing past activity at Sangay and El Reventador, where no local infrasound monitoring was available during the period of the analysis covered here. We show that hierarchical clustering together with the Ward's criterion can help to retrieve impulsive signals and automate signal detection in a multiyear data set from a single infrasound array. Additionally, we highlight the utility of ground-based regional infrasound monitoring to detect eruptions in Ecuador. The cross bearings approach applied to data from LITE and RIOE show that eruptions that are not detected by MODVOLC can be tracked regionally using theses infrasound arrays. Lastly, we observe that factors such as wind noise, source-receiver range, and eruption sizes can affect our ability to detect eruptions of Ecuadorian volcanoes at regional scales (~15-250 km ranges).

ACKNOWLEDGMENTS

We used data from the Acoustic Surveillance for Hazardous Eruptions (ASHE) project (McCormack et al., 2005; Garcés et al., 2008); we thank Tim Côté and Xiuying Jin of Natural Resources Canada (NRCan) for facilitating our data archive request. The PMCC software are provided by CEA (Cansi, 1995). This work was supported by NSF grant EAR-1847736.

APPENDIX A

A detail information about the Ward's criterion can be found in Ward (1963) and Murtagh and Legendre (2014). Here we summarize the backbone of the Ward's algorithm following these references.

The Ward's criterion is a general agglomerative hierarchical clustering method that seeks to minimize a define objective function in each step, where a pair of clusters is merge. The most common objective function used in the literature and in recent software packages (e.g. R Core Team, 2020; https://www.R-project.org/) is the error sum of squares. As result the Ward's criterion is often referred as the Ward's minimum variance method. The workflow is: at the initial step all clusters have one element, then for each step the algorithm merges two clusters that minimize the total variance of the combined cluster, and repeat until grouping all elements.

REFERENCES

Albert, S., & Linville, L. (2020). Benchmarking Current and Emerging Approaches to Infrasound Signal Classification. Seismological Research Letters, 91, 921–929. https://doi.org/10.1785/0220190116

Almeida, M., Gaunt, H., & Ramón, P. (2019). Ecuador's El Reventador volcano continually remakes itself, Eos, 100.

Anderson, J., Johnson, J., Bowman, D., & Ronan, T. (2018). The Gem infrasound logger and custom-built instrumentation. Seismological Research Letters, 89, 153–164. https://doi.org/10.1785/0220170067

Anderson, J., Iezzi, A., Fee, D., Johnson, J., Waite, G., Matoza, R., McKee, K., & Arrowsmith, S. (2020). Infrasound needs from a future geophysical facility, White paper for Competition of Operations of an NSF-supported Geophysical Facility to Succeed the GAGE and SAGE Facilities.

Anzieta, J.C., Ortiz, H.D., Arias, G.L., & Ruiz, M.C. (2019). Finding Possible Precursors for the 2015 Cotopaxi Volcano Eruption Using Unsupervised Machine Learning Techniques. International Journal of Geophysics. https://doi.org/10.1155/2019/6526898

Arellano, S.R., Hall, M., Samaniego, P., Le Pennec, J.L., Ruiz, A., Molina, I., & Yepes, H. (2008). Degassing patterns of Tungurahua volcano (Ecuador) during the 1999–2006 eruptive period, inferred from remote spectroscopic measurements of SO2 emissions. Journal of Volcanology and Geothermal Research, 176 (1), 151–162. https://doi.org/10.1016/j.jvolgeores.2008.07.007

Arnold, D. W. D., Biggs, J., Anderson, K., Vallejo, S., Wadge, G., Ebmeier, S. K., Naranjo, M., & Mothes, P. (2017). Decaying lava extrusion rate at El Reventador Volcano, Ecuador, measured using high-resolution satellite radar. Journal of Geophysical Research: Solid Earth, 122, 9966–9988. https://doi.org/10.1002/2017JB014580

Arnold, D.W.D., Biggs, J., Dietterich, H.R., Vargas, S.V., Wadge, G., & Mothes, P. (2019). Lava flow morphology at an erupting andesitic stratovolcano: A satellite perspective on El Reventador, Ecuador. Journal of Volcanology and Geothermal Research. 372, 34–47. https://doi.org/10.1016/j.jvolgeores.2019.01.009

Arrowsmith, S. J., Johnson, J. B., Drob, D. P., & Hedlin, M. A. (2010). The seismoacoustic wavefield: A new paradigm in studying geophysical phenomena. Reviews of Geophysics, 48(4). https://doi.org/10.1029/2010RG000335

Assink, J. D., Waxler, R., & Drob, D. (2012). On the sensitivity of infrasonic traveltimes in the equatorial region to the atmospheric tides. Journak of Geophysical Research, 117, D01110. https://doi.org/10.1029/2011JD016107

Cannata, A., Montalto, P., Aliotta, M., Cassisi, C., Pulvirenti, A., Privitera, E., & Patanè, D. (2011). Clustering and classification of infrasonic events at Mount Etna using pattern recognition techniques. Geophysical Journal International, 85(1), 253–264.

Cansi, Y. (1995). An automatic seismic event processing for detection and location: The P.M.C.C. method. Geophysical Research Letters, 22(9), 1021 – 1024. https://doi.org/10.1029/95GL00468

Cansi Y., & Le Pichon A. (2008). Infrasound Event Detection Using the Progressive Multi-Channel Correlation Algorithm. In: Havelock D., Kuwano S., Vorländer M. (eds) Handbook of Signal Processing in Acoustics. Springer, New York, NY. https://doi.org/10.1007/978-0-387-30441-0 77

Fee, D., Garcés, M., & Steffke, A. (2010). Infrasound from Tungurahua Volcano 2006–2008: Strombolian to Plinian eruptive activity. Journal of Volcanology and Geothermal Research, 193(1–2). https://doi.org/10.1016/j.jvolgeores.2010.03.006

Fee, D., Johnson, J., Lyons, J., Haney, M., & Matoza, R. (2020). Community Network for Volcanic Eruption Response (CONVERSE) – Infrasound Workshop Report, NSF Research Coordination Network (RCN).

Garcés, M., Fee, D., Steffke, A., McCormack, D., Servranckx, R., Bass, H., Hetzer, C., Heldin, M., Matoza, R., Yepes, H., & Ramon, P. (2008). Capturing the acoustic fingerprint of stratospheric ash injection. Eos, 89 https://doi.org/10.1029/2008EO400001

Grangeon, J., & Lesage, P. (2019). A robust, low-cost and well-calibrated infrasound sensor for volcano monitoring. Journal of Volcanology and Geothermal Research, 387, 106668. https://doi.org/10.1016/j.jvolgeores.2019.106668

Hall, M., Ramón, P., Mothes, P., LePennec J., Garcia, A., Samaniego, P., & Yepes, H. (2004). Volcanic eruptions with little warning: the case of Volcan Reventador's Surprise November 3, 2002 Eruption, Ecuador. Revista Geológica de Chile, 31 (2), 349–358. http://dx.doi.org/10.4067/S0716-02082004000200010

Ham, F. M., & Park, S. (2002). A robust neural network classifier for infrasound events using multiple array data. Proceedings of the 2002 International Joint Conference on Neural Networks, 3, 2615–2619. http://dx.doi.org/10.1109/IJCNN.2002.1007556

Hedlin, M. A. H., Walker, K., Drob, D. P., & de Groot-Hedlin, C. D. (2012). Infrasound: Connecting the solid earth, oceans, and atmosphere. Annual Review of Earth and Planetary Sciences, 40, 327-354. https://doi.org/10.1146/annurev-earth-042711-105508

Hidalgo, S., Battaglia, J., Arellano, S., Steele, A., Bernard, B., Bourquin, J., Galle, B., Arrais, S., & Vásconez, F. (2015). SO2 degassing at Tungurahua volcano (Ecuador) between 2007 and 2013: transition from continuous to episodic activity. Journal of Volcanology and Geothermal Research, 298, 1–14. https://doi.org/10.1016/j.jvolgeores.2015.03.022

Johnson, J.B., Lees, J.M. (2000). Plugs and chugs - seismic and acoustic observations of degassing explosions at Karymsky, Russia and Sangay, Ecuador. Journal of Volcanology and Geothermal Research, 101, 67–82.

Kong, Q., Trugman, D., Ross, Z., Bianco, M., Meade, B., & Gerstoft, P. (2019). Machine Learning in Seismology: Turning Data into Insights. Seismological Research Letters, 90(1), 3–14. https://doi.org/10.1785/0220180259

Lees, J.M., Ruiz, M. (2008). Non-linear explosion tremor at Sangay, Volcano, Ecuador. Journal of Volcanology and Geothermal Research, 176, 170–178. https://doi.org/10.1016/j.jvolgeores.2007.08.012

Le Pichon, A., Blanc, E., and Hauchecorne, A. (2019). Infrasound Monitoring for Atmospheric Studies, Springer, Dordrecht Heidelberg London New York. https://doi.org/10.1007/978-3-319-75140-5

Li, M., Liu, X., & Liu X. (2016). Infrasound signal classification based on spectral entropy and support vector machine. Applied Acoustics, 113, 116–120. https://doi.org/10.1016/j.apacoust.2016.06.019

Liu, X., Li, M., Tang, W., Wang, S., & Wu, X. (2014). A new classification method of infrasound events using Hilbert-Huang transform and support vector machine. Mathematical Problems in Engineering, 456818. https://doi.org/10.1155/2014/456818

Marcillo, O., Johnson, J. B., & Hart, D. (2012). Implementation, characterization, and evaluation of an inexpensive low-power low-noise infrasound sensor based on a micro-machined differential pressure transducer and a mechanical filter. Journal of Atmospheric and Oceanic Technology, 29(9), 1275–1284. https://doi.org/10.1175/JTECH-D-11-00101.1

Matoza, R.S., Fee, D., Garcés, M., Seiner, J., Ramón, P., & Hedlin, M. (2009). Infrasonic jet noise from volcanic eruptions, Geophysical Research Letters, 36, L08303. https://doi.org/10.1029/2008GL036486

Matoza, R.S., Fee, D., Neilsen, T., Gee, K., & Ogden, D. (2013). Aeroacoustics of volcanic jets: Acoustic power estimation and jet velocity dependence. Journal of Geophysical Research: Solid Earth, 118, 6269-6284. https://doi.org/10.1002/2013JB010303

Matoza, R.S., & Fee, D. (2014a). Infrasonic component of volcano-seismic eruption tremor. Geophysical Research Letters, 41, 1964-1970. https://doi.org/10.1002/2014GL059301

Matoza, R.S., Fee, D., & Lopez, T. (2014). Acoustic characterization of explosion complexity at Sakurajima, Karymsky, and Tungurahua Volcanoes. Seismological Research Letters, 85, 6, 1187-1199. https://doi.org/10.1785/0220140110

Matoza, R.S., Green, D., Le Pichon, A., Shearer, P., Fee, D., Mialle, P., & Ceranna L. (2017). Automated detection and cataloging of global explosive volcanism using the International Monitoring System infrasound network. Journal of Geophysical Research: Solid Earth, 122, 2946–2971. https://doi.org/10.1002/2016JB013356

Matoza, R.S., Fee, D., Green, D., Le Pichon, A., Vergoz, J., Haney, H., Mikesell, T. D., Franco, F., Valderrama, A., Kelley, M., McKee, K., & Ceranna, L. (2018). Local, regional, and remote seismo-acoustic observations of the April 2015 VEI 4 eruption of Calbuco volcano, Chile. Journal of Geophysical Research: Solid Earth, 123, 3814–3827. https://doi.org/10.1002/2017JB015182

Matoza, R.S., & Fee, D., (2018). The inaudible rumble of volcanic eruptions. Acoustics Today, 14:1, 17-25, Spring 2018

Matoza, R., Fee, D., Green, D., & Mialle, P. (2019). Volcano infrasound and the International Monitoring System, in "Infrasound monitoring for atmospheric studies: Challenges in middle-atmosphere dynamics and societal benefits", ed. A. Le Pichon, E. Blanc, and A. Hauchecorne, Ch 33, pp 1023-1077, Springer. https://doi.org/10.1007/978-3-319-75140-5

Marty, J. (2019). The IMS infrasound network: current status and technological developments, in "Infrasound monitoring for atmospheric studies: Challenges in middle-atmosphere dynamics and societal benefits", ed. A. Le Pichon, E. Blanc, and A. Hauchecorne, Ch 1, pp 3-62, Springer. https://doi.org/10.1007/978-3-319-75140-5

McCormack, D., Bass, H., Garcés, M., & Yepes, H. (2005). Acoustic surveillance for hazardous eruptions (ASHE). The Journal of the Acoustical Society of America, 117(4), 2419-2419. https://doi.org/10.1121/1.4786426

Monzier, M., Robin, C., Samaniego, P., Hall, M., Cotten, J., Mothes, P., & Arnaud N. (1999). Sangay volcano, Ecuador: Structural development, present activity and petrology. Journal of Volcanology and Geothermal Research, 90(1), 49–79.

Mothes, P., Yepes, H., Hall, M., Ramón, P., Steele, A., & Ruiz, M. (2015). The scientific-community interface over the fifteen-year eruptive episode of Tungurahua Volcano, Ecuador. Journal of Applied Volcanology. 4, 9.

Murtagh, F., & Legendre, P. (2014). Ward's Hierarchical Agglomerative Clustering Method: Which Algorithms Implement Ward's Criterion? Journal of Classification, 31, 274–295. https://doi.org/10.1007/s00357-014-9161-z

Naranjo, M.F., Ebmeier, S.K., Vallejo, S., Ramón P., Mothes P., Biggs, J., & Herrera F. (2016). Mapping and measuring lava volumes from 2002 to 2009 at El Reventador Volcano, Ecuador, from field measurements and satellite remote sensing. Journal of Applied Volcanology. 5, 8. https://doi.org/10.1186/s13617-016-0048-z

Ortiz, H. D., Johnson, J. B., Ramón, P., & Ruiz, M. C. (2018). Using infrasound waves to monitor tropospheric weather and crater morphology changes at Tungurahua Volcano, Ecuador. Journal of Volcanology and Geothermal Research.

Ortiz, H. D., Johnson, J. B., Anzieta, J. C., Matoza, R. S., Anderson, F. J., Vallejo S., Cordova, J. A., Ruiz, M. C., Naranjo, M. F., Ramón, P., and Hernandez S. (2019). Overview of Reventador infrasound Activity: from January 2015 to June 2019. Abstract V44B-06 presented at 2019 Fall Meeting, San Francisco, CA, 9-13 Dec.

Ortiz, H. et al. (2018). Caracterización y estadística de señales volcánicas en los Andes, casos de estudio volcanes Reventador y Cotopaxi en Ecuador. Revista Geofísica, (68), 119-123. https://doi.org/10.35424/rgf.v0i68.938

Ortiz H. D., Matoza R. S., Johnson J. B., Hernandez S., Anzieta J. C., and Ruiz M. C. (2021). Autocorrelation infrasound interferometry. Journal of Geophysical Research: Solid Earth.

Park, S., Ham, F., & Lowrie, C. (2005). Discrimination of infrasound events using parallel neural network classification banks. Nonlinear Analysis: Theory, Methods & Applications, 63(5–7), e859–e865. https://doi.org/10.1016/j.na.2005.02.016

Robles, A. (2010). Cambios morfologicos y medidas termicas en los flancos superiors del volcan Sangay, desde el año 2003 hasta el presente. Escuela Politécnica Nacional.

Ruiz, M.C., Lees, J.M. & Johnson, J.B. (2006). Source constraints of Tungurahua volcano explosion events. Bulletin of Volcanology, 68, 480–490 (2006). https://doi.org/10.1007/s00445-005-0023-8

Sanderson, R. W., Matoza, R. S., Fee, D., Haney, M. M., & Lyons, J. J. (2020). Remote detection and location of explosive volcanism in Alaska with the EarthScope transportable array. Journal of Geophysical Research: Solid Earth, 125

Shani-Kadmiel, S., Assink, J. D., Smets, P. S., & Evers, L. G. (2018). Seismoacoustic coupled signals from earthquakes in central Italy: Epicentral and secondary sources of infrasound. Geophysical Research Letters, 45(1), 427-435.

Szuberla, C.A.L., & Olson, J.V. (2004). Uncertainties associated with parameter estimation in atmospheric infrasound arrays. Journal of the Acoustical Society of America, 115 (1), 253–258. https://doi.org/10.1121/1.1635407

Walker K.T., Hedlin M.A. (2010). A Review of Wind-Noise Reduction Methodologies. In: Le Pichon A., Blanc E., Hauchecorne A. (eds) Infrasound Monitoring for Atmospheric Studies. Springer, Dordrecht. https://doi.org/10.1007/978-1-4020-9508-5 5

Ward, J.H. (1963). Hierarchical Grouping to Optimize an Objective Function. Journal of the American Statistical Association, 58, 236–244. https://doi.org/10.1080/01621459.1963.10500845

Watson L., (2020). Using unsupervised machine learning to identify changes in eruptive behavior at Mount Etna, Italy. Journal of Volcanology and Geothermal Research, 405. https://doi.org/10.1016/j.jvolgeores.2020.107042.

Wilson, D. C., Davis, P., Ebeling, C., Hutt, C. & Hafner, K. (2018). Seismic sensors record a hurricane's roar, Eos, 99.

Witsil, A., & Johnson, J. (2020). Analyzing continuous infrasound from Stromboli volcano, Italy using unsupervised machine learning. Computers & Geosciences, Volume 140. https://doi.org/10.1016/j.cageo.2020.104494

Wright, R., Flynn, L. P., Garbeil, H., Harris, A. J. L. & Pilger, E. (2002). Automated volcanic eruption detection using MODIS. Remote Sensing of Environment, 82, 135–155. https://doi.org/10.1016/S0034-4257(02)00030-5

Wright, R., Flynn, L.P., Garbeil, H., Harris, A.J.L., & Pilger, E. (2004). MODVOLC: Near-real-time thermal monitoring of global volcanism. Journal of Volcanology and Geothermal Research, 135, 29–49. https://doi.org/10.1016/j.jvolgeores.2003.12.008